



HAL
open science

Influence of thickness and microstructure on thermoelectric properties of Mg-doped CuCrO₂ delafossite thin films deposited by RF-magnetron sputtering

Inthuga Sinnarasa, Yohann Thimont, Lionel Presmanes, Corine Bonningue, Antoine Barnabé, Philippe Tailhades

► To cite this version:

Inthuga Sinnarasa, Yohann Thimont, Lionel Presmanes, Corine Bonningue, Antoine Barnabé, et al.. Influence of thickness and microstructure on thermoelectric properties of Mg-doped CuCrO₂ delafossite thin films deposited by RF-magnetron sputtering. *Applied Surface Science*, 2018, 455, pp.244-250. 10.1016/j.apsusc.2018.05.104 . hal-02335643

HAL Id: hal-02335643

<https://hal.science/hal-02335643>

Submitted on 28 Oct 2019

HAL is a multi-disciplinary open access archive for the deposit and dissemination of scientific research documents, whether they are published or not. The documents may come from teaching and research institutions in France or abroad, or from public or private research centers.

L'archive ouverte pluridisciplinaire **HAL**, est destinée au dépôt et à la diffusion de documents scientifiques de niveau recherche, publiés ou non, émanant des établissements d'enseignement et de recherche français ou étrangers, des laboratoires publics ou privés.



Open Archive Toulouse Archive Ouverte (OATAO)

OATAO is an open access repository that collects the work of Toulouse researchers and makes it freely available over the web where possible

This is an author's version published in: <http://oatao.univ-toulouse.fr/24522>

Official URL: <https://doi.org/10.1016/j.apsusc.2018.05.104>

To cite this version:

Sinnarasa, Inthuga^{ORCID} and Thimont, Yohann^{ORCID} and Presmanes, Lionel^{ORCID} and Bonningue, Corine^{ORCID} and Barnabé, Antoine^{ORCID} and Tailhades, Philippe^{ORCID}
Influence of thickness and microstructure on thermoelectric properties of Mg-doped CuCrO₂ delafossite thin films deposited by RF-magnetron sputtering.
(2018) Applied Surface Science, 455. 244-250. ISSN 0169-4332

Any correspondence concerning this service should be sent to the repository administrator: tech-oatao@listes-diff.inp-toulouse.fr

Influence of thickness and microstructure on thermoelectric properties of Mg-doped CuCrO₂ delafossite thin films deposited by RF-magnetron sputtering

Inthuga Sinnarasa, Yohann Thimont*, Lionel Presmanes, Corine Bonningue, Antoine Barnabé, Philippe Tailhades

CIRIMAT, Université de Toulouse, CNRS, INPT, Université Paul Sabatier, 118 Route de Narbonne, 31062 Toulouse Cedex 9, France

ARTICLE INFO

Keywords:

Thermoelectric thin film
Microstructure/thickness dependence
Delafossite
Radio-frequency sputtering
Hopping transport

ABSTRACT

Thermoelectric thin films are of great interest to microelectronic devices and miniaturized temperature sensors. In this article, we have studied the influence of film thickness on the electrical and thermoelectric properties of Mg-doped CuCrO₂ delafossite material (CuCrO₂:Mg), a delafossite-type oxide. For this purpose, a series of CuCr_{0.97}Mg_{0.03}O₂ thin films with various thicknesses (25, 50, 100, 200, 300, 400 and 600 nm) have been deposited by Radio Frequency (RF) magnetron sputtering. The as-deposited films were annealed at 550 °C under vacuum to obtain well crystallized delafossite phase. Grazing incidence X-ray diffraction patterns indicated that samples had pure delafossite structure. The atomic force microscope observations revealed the increase of the grain size with increasing thickness. The electrical and thermoelectric properties are characterized in temperature ranging from 40 to 220 °C and they were thickness dependent. The thickness dependency of the Seebeck coefficient was not expected and indicated that the carrier density changes with thickness below 100 nm. The variation of the film resistivity below 100 nm thickness was explained by both the change of the carrier density and the potential barrier addition due to small grain size. Using the electrical conductivity, the polaron activation energy ($E_{op} = 0.131$ eV for 100 nm thick sample) was determined and its variation indicated that the stress/strain effect in the film with increasing thickness impacts the mobility. Moreover, the unexpected increase of the resistivity between 400 and 600 nm was also explained by the micro-cracks formation. The electrical and thermoelectric measurements showed a degenerated hopping semi-conductor behavior for the whole thicknesses. The highest electrical conductivity (1.7 S \cdot cm⁻¹ at 40 °C) was obtained for 100 nm thick film which presented a Seebeck coefficient of $+307$ μ V \cdot K⁻¹ at 40 °C. We report maximum power factor of 16 μ W \cdot m⁻¹·K⁻² at 40 °C for the optimum thickness of 100 nm, which reached 59 μ W \cdot m⁻¹·K⁻² at 200 °C. The above results were explained in terms of microstructure and stress/strain effect.

1. Introduction

Recent attention has been focused on the CuMO₂ delafossite oxide family where the cation Cu^I is a monovalent metal and the cation M^{III} is a trivalent metal. The delafossite structure can be described as a stack of cation Cu^I layer and MO₆ octahedron layer along the c axis. Each cation Cu^I is linearly coordinated to two oxygens belonging to upper and lower MO₆ octahedron. Among Cu based delafossites, CuCrO₂ is currently of interest due to its attractive physical properties and the abundance of their constituent elements in the nature. Thanks to its transparent p type conduction properties (TCO) [1–12], it has been studied for several applications such as transparent electronic devices [13–17], dye sensitized solar cells [18,19] and photoelectrodes [20]. This

material is also outstanding for its catalysis [21] and photo catalysis [21–26], antibacterial [27], gas and sensing [28–31], energy storage [32], water reduction [33], superconductivity [34], magnetic and electric [35–37] outstanding properties. Interesting thermoelectric (TE) properties [38–44] have also been reported in the last decade due to its high Seebeck coefficient.

The thermoelectricity defines as a direct and reciprocal energy conversion between the temperature differences and the electric voltage. The performance of TE materials are evaluated with the figure of merit ($ZT = S\sigma T/\kappa$) where S is the Seebeck coefficient, σ is the electrical conductivity and κ is the thermal conductivity). Materials with high ZT ($ZT \geq 1$) are necessary in order to be used in TE devices. Thermoelectric properties are widely studied in bulk form compared to

* Corresponding author.

E-mail address: thimont@chimie.ups-tlse.fr (Y. Thimont).

thin film. However, for some TE applications, such as flexible temperature sensor [45–47], fiber optic switches [48], small scale power generation applications [49], large area transparent thin film thermoelectric devices [50,51], hot spot (H S) cooling [52] and on chip energy harvesting [53], TE materials are required in thin film form. In particular, metal oxide semiconductor processing technology facilitates mass production of low cost thin film thermoelectric devices for thermal management and control. These embeddable TE modules made with semiconductor processing techniques have high heat pumping capability in comparison with standard bulk TE modules and enable a very rapid cooling and heating for a precise temperature control [54].

Furthermore, TE materials in thin film form offer the possibility to enhance ZT values due to specific microstructures which can lead to a significant reduction of the thermal conductivity relative to that observed in bulk material [55–58]. These microstructural effects can however reduce the electrical conductivity by increasing scattering effects, and a compromise between the thermal conductivity and the electrical conductivity is then necessary to increase ZT. Moreover, the low dimension system and the strains obtained in thin films due to the substrate could make a significant band structure modification that could impact the figure of merit.

In order to optimize TE materials, the first approach is the enhancement of the Power Factor ($PF = \sigma S^2$). This can be done by optimizing the carrier concentration by doping [39], the mobility by tuning the microstructure [59,60]. In a previous work [61], we studied the electrical conductivities and TE properties (Seebeck coefficient and calculated power factor) in temperature from 40 °C to 220 °C for one set of CuCrO_2 films annealed at various temperatures, with a thickness of 300 nm. We noticed that the annealing temperature affected a lot the films microstructure and the physical properties. The optimal annealing temperature under primary vacuum was found to be 550 °C. In order to find the optimal thickness for a higher PF which is rarely investigated for oxide thin films, in the present work, we have studied the relation between the TE properties of $\text{CuCr}_{0.97}\text{Mg}_{0.03}\text{O}_2$ thin films and the thickness through microstructural effects. For that, samples with various thicknesses (25, 50, 100, 200, 300 and 400 nm) have been deposited and then annealed at 550 °C (the optimal annealing temperature found in the previous study) under vacuum.

2. Experimental

2.1. Preparation of Mg doped CuCrO_2 (Target)

Polycrystalline $\text{CuCr}_{0.97}\text{Mg}_{0.03}\text{O}_2$ powder was prepared by grinding and mixing the starting commercial oxides, Cu_2O , Cr_2O_3 , and MgO with appropriate proportions. The stoichiometric oxide mixture was annealed at 900 °C for 10 h in an ambient nitrogen atmosphere and cooled down to room temperature. After it was reground, the mixture was reheated for a further 10 h period. The purity of the delafossite phase was checked by X Ray Diffraction (XRD).

The polycrystalline delafossite powder has been pressed into a sputtering target of 10 cm in diameter then sintered at 1200 °C for 10 h in air (diameter after sintering : 8.7 cm). The XRD analysis on a small representative pellet showed only the 3R delafossite phase. (R 3m space group with $a = 2.9755(2)$ Å and $c = 17.091(3)$ Å as determined by the Rietveld method).

2.2. Preparation of Mg doped CuCrO_2 thin films

In order to deposit $\text{CuCr}_{0.97}\text{Mg}_{0.03}\text{O}_2$ thin films, the target assembly was attached to an Alcatel A450 RF magnetron sputtering chamber (Alcatel, France). Fifteen minutes of pre sputtering with argon plasma has been applied before starting the film deposition to remove the surface contamination. Pre cleaned fused silica substrates (25 mm × 25 mm, ≈1 mm thick) placed on a water cooled sample holder were used during the deposition. In order to avoid the reduction

Table 1

Process parameters for the deposition of delafossite Mg-doped CuCrO_2 by RF-sputtering.

Target material	3 at % Mg-doped CuCrO_2
Substrate	Fused silica
Power (W)	50
Magnetron	Yes
Argon pressure P (Pa)	0.5
Target to substrate distance d (cm)	5

of the target, a low argon pressure [62] was used during the sputtering process. The deposition parameters are summarized in the Table 1. Under these conditions, as deposited films with normalized thickness of 25, 50, 100, 200, 300, 400 and 600 nm have been elaborated. The X ray fluorescence (XRF) measurement (not shown here) carried out with a Bruker S2 apparatus showed that the ratio was close to 1 Cu for 1 Cr in the film (with accuracy range of 5%) which is consistent with the composition of the target ($\text{CuCr}_{0.97}\text{Mg}_{0.03}\text{O}_2$).

The as deposited films have been systematically annealed for 4 h under primary vacuum at 550 °C.

2.3. Characterization

Thickness measurements were performed with a DEKTAT 3030ST profilometer, before and after the thermal treatment, on a step made by applying a tape on the substrate surface prior to the sputtering step. The structural properties of the films were investigated by a $\alpha = 1^\circ$ grazing incidence X ray diffraction (GIXRD) at room temperature. GIXRD was performed using a Siemens D5000 diffractometer equipped with a Bruker Sol X detector (Siemens, USA). Copper radiations were used as X ray source ($\lambda_{\text{CuK}\alpha 1} = 1.5405$ Å and $\lambda_{\text{CuK}\alpha 2} = 1.5445$ Å). The microstructure of the films was observed using a Joel JSM7800F field emission gun Scanning Electron Microscope (SEM) and an optical microscope S Neox and a Nanoscope III Dimension 3000 Atomic Force Microscope (AFM). AFM surface views were analyzed using the Gwyddion software.

The electrical resistivity was measured using a four point probe measurement unit (Signatone, USA).

A home made measurement setup has been used for the Seebeck coefficient determination as a function of temperature. Two independent heaters fitted to the thin film geometry have been used to apply a thermal gradient along the thin film. Electrical contacts were done with a 25 μm diameter aluminum wire bonder (HYBOND Model 626, Hybond, USA). The ohmic type behavior (linearity of current vs. voltage curve) of the electrical contacts has been checked systematically for all samples with a source meter (Keithley 2450, Tektronix, USA) after bonding step. During the experiment, the voltage was measured with a nanovoltmeter (Keithley 2182A, Tektronix, USA). Two carbon spots (emissivity coefficient of 0.97) were deposited on the surface of the thin films by spraying carbon solution through a shadow mask to accurately measure the surface temperature with an infrared camera. The two carbon spots were located at the same isotherm position than the electrical contacts. The mean temperature (T_{Mean}) was considered as the average between the temperature of the hot side (T_{Hot}) and that of the cold side (T_{Cold}). To have a good accuracy, three measurements of electric potentials and temperatures for a given temperature difference are done. For each Seebeck coefficient, three temperature differences was applied (10, 20 and 30 °C).

The Seebeck coefficient $S(T_{\text{Mean}})$ at a given mean temperature can be calculated with:

$$S(T_{\text{mean}}) = S_{\text{ref}} - \frac{\Delta V}{\Delta T} \quad (1)$$

where S_{ref} , ΔV , and ΔT are respectively Seebeck coefficient of the reference (Aluminum probe is used as reference whose Seebeck

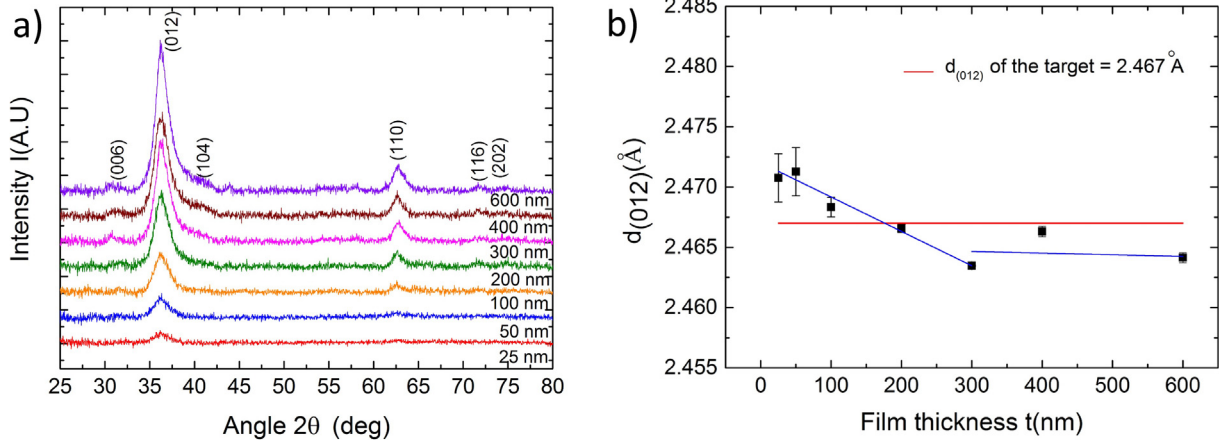


Fig. 1. (a) GIXRD patterns of $\text{CuCrO}_2\text{:Mg}$ thin films annealed at 550°C under vacuum. (b) $d_{(012)}$ as a function of the film thickness.

coefficient is negligible because Fermi energy level of aluminum is near the middle of the energy band), electric potential and temperature difference ($T_{\text{Hot}} - T_{\text{Cold}}$) measured on the film. The accuracy of the experimental setup was checked by using a bar of $\text{Ca}_3\text{Co}_4\text{O}_9$ already measured elsewhere with a ZEM3 commercial apparatus. The results were similar with a standard deviation of 7%.

3. Results and discussion

3.1. Structural and microstructural characterizations

First, we examined the crystal structure of $\text{CuCrO}_2\text{:Mg}$ thin films annealed at 550°C for 4 h under vacuum. The Fig. 1a shows the GIXRD patterns of the annealed films for various thicknesses. For 25 and 50 nm thick films, the intensity of the GIXRD signal was not significant due to the insufficient quantity of matter (large standard deviation on the peak position). Beyond 100 nm, peaks characteristics of the delafossite structure (006), (012), (110), (104), (116) and (202) appeared progressively with increasing film thickness. These diffraction peaks matched well with 3R delafossite phase pattern (PC PDF file #39 0247). Only delafossite phase has been observed for whole studied thicknesses. It is difficult to identify any impurity peak due to the width of the strongest diffraction peak. The (006) peak is weakly represented in adequacy with works on the delafossite CuCrO_2 films [5,63].

The Fig. 1b shows the distance between the planes (012) as a function of the film thickness. For 25 and 50 nm thick films, the accuracy is poor due to a large and not intense X ray diffraction peak. Even if the values of $d_{(012)}$ are closed to the distance calculated with the target lattice parameters, the value of $d_{(012)}$ tends to decrease when the thickness increases from 25 nm to 300 nm and seems stabilized above 300 nm. This tendency reveals the strain accumulation in the delafossite structure with increasing thickness because of the lower thermal expansion coefficient of the fused silica ($0.5 \times 10^{-6} \text{ K}^{-1}$) [64] in comparison with the film. Beyond 300 nm, the stabilization of $d_{(012)}$ shows that the film starts to relax the strain probably by the micro cracks which is magnified at 600 nm as shown in the Fig. 2b and c.

The AFM micrographs of $\text{CuCrO}_2\text{:Mg}$ thin films (Fig. 2a) show smooth surface at 25 nm and 50 nm, while granular layer could be observed for the higher thicknesses (100–600 nm). The grains were marked using watershed algorithm to estimate the grain size. It was observed that the surface grain diameter increased with the film thickness, the 100, 200 and 400 nm thick films have respectively 16, 23 and 32 nm grain size. The 600 nm film shows a different morphology where the small grains (25 nm) form large clusters (91 nm) with a very high roughness which can be due to a partial stress relaxation of the film. The Fig. 2b shows the top surface SEM micrographs of the 600 nm annealed film. The surface morphology of this sample is consistent with

the morphology observed by AFM and shows a large crack. The Fig. 2c shows optical microscope image of the 600 nm thick film and allows to see wider. The film presents several micro cracks at the surface. For thinner films, the cracks could not be observed so it confirms the presence of tensile stress could not be relaxed when samples were cooled down from 550°C during the thermal annealing.

3.2. Electrical and thermoelectric properties analysis

3.2.1. Seebeck coefficient analysis

The Seebeck coefficient values are positive for whole studied thicknesses as shown in the Fig. 3. It indicates the p type conduction, in agreement with the literature [1,39,65].

The Seebeck coefficient versus temperature (Inset Fig. 3) for a given thin film thickness remains constant and corresponds to constant Fermi level location from the top of the valence band [61] with the temperature. It is in agreement with a highly degenerated semiconductor behavior. It is also determined by the slope of the Seebeck coefficient as a function of the logarithm of the electrical conductivity for various temperatures (Fig. 3) called Jonker plot which are not equal to $k_B/e = 86.15 \mu\text{V}\cdot\text{K}^{-1}$ (where k_B is Boltzmann's constant and e is the electronic charge). The Seebeck and the electrical conductivity (discussed afterward) behavior as function of the temperature is in agreement with highly degenerated hopping semiconductor properties. In fact, the electrical conductivity increased with the temperature while the Seebeck coefficient stays constant. In the case of band gap semiconductor with free holes in the valence band, the Seebeck coefficient will decrease with the temperature. Only hopping mechanism can explain simultaneously Seebeck and electrical conductivity behavior with the temperature in this material.

Moreover, the band gap of $\text{CuCrO}_2\text{:Mg}$ is about 2.73 eV [61] which is high enough for TCO applications and avoids the band gap electronic transition. Indeed, if the band gap electronic transition was possible, the presence of the both carrier types could lead to a very low global Seebeck coefficient ($S_T = (\sigma_n S_n + \sigma_p S_p)/(\sigma_n + \sigma_p)$, where σ_p and S_p are respectively the electrical conductivity and the Seebeck coefficient due to the holes σ_n and S_n are respectively the electrical conductivity and the Seebeck coefficient due to the electrons.). In our case, the carrier concentration does not depend of the temperature in a large range ($10 k_B T < E_g$).

The hole density is deduced from the Heikes relation which is well adapted in the case of hopping mechanism:

$$S = \frac{k_B}{e} \times \ln \left(a \times \frac{[\text{Cu}^+]}{[\text{Cu}^{2+}]} \right) \quad (2)$$

where a is a constant which depends of the spin and orbital degeneracy and is equal to $\frac{1}{4}$ in the case of CuCrO_2 structure. Seebeck

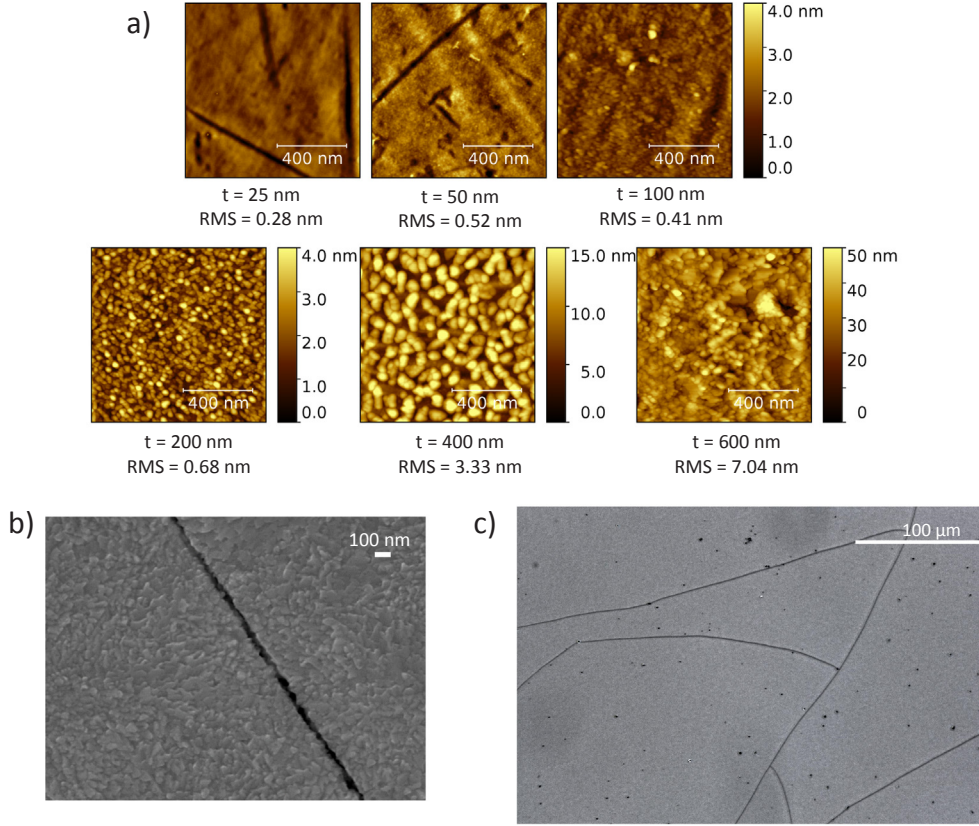


Fig. 2. (a) AFM micrographs of the annealed $\text{CuCrO}_2\text{:Mg}$ films. (b) Top surface SEM micrograph and (c) optical microscope image of the 600 nm annealed film.

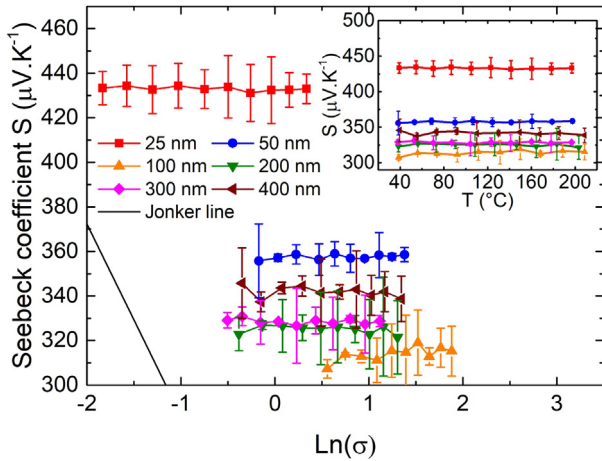


Fig. 3. Jonker plot. Inset: Seebeck coefficient as a function of measuring temperature.

coefficient is then only dependent of the $[\text{Cu}^+]/[\text{Cu}^{2+}]$ ratio where $[\text{Cu}^{2+}]$ is equal to the hole concentration. This ratio is defined by the dopant (Mg^{2+}) concentration and oxygen non stoichiometry.

The measured Seebeck coefficient is thickness dependent. It decreased from 25 nm to 100 nm then it is stabilized for films thicknesses above 100 nm. Even 600 nm thick film which presented cracks at the surface, shows a Seebeck coefficient of $300 \mu\text{V} \cdot \text{K}^{-1}$ at 220°C (not shown in the Fig. 3). Seebeck coefficient is an intrinsic property of the material (Fermi level variation in the case of semiconductors) and relates to the carrier concentration in the case of the hopping mechanism. We can conclude that the carrier concentration increases from $3.85 \times 10^{19} \text{ cm}^{-3}$ to a nearly saturated value of $1.25 \times 10^{20} \text{ cm}^{-3}$ calculated respectively from the Seebeck coefficient of the 25 nm thick

film and the Seebeck coefficient of the film with higher thickness than 100 nm. Lunca Popa et al. [66] have also calculated the carrier concentration using the small polaron transport model and obtained $1.5 \times 10^{21} \text{ cm}^{-3}$ for 200 nm Mg doped CuCrO_2 film.

This unexpected variation of the carrier concentration for low thicknesses which is related to the dopant concentration and oxygen non stoichiometry, is not clearly understood. However, the following hypotheses can be used as an explanation:

The influence of the structural lattice deformations due to the stress induced by the substrate which is compressive in the case of low films thicknesses as shown by the highest $d_{(012)}$ noticed by XRD (Fig. 1b).

An incomplete crystallization of the delafossite structure similar to the effect of a low temperature thermal annealing studied in a previous article [61].

For thicknesses above 100 nm, no clear variation of the Seebeck coefficient and consequently, the hole concentration was identified. We can conclude that crystallization of the delafossite structure and the doping are stable above 100 nm.

3.2.2. Electrical resistivity analysis

The Fig. 4a reports the electrical resistivity at room temperature as a function of the film thickness. The observed behavior of the electrical resistivity is not representative in comparison with the classical film resistivity variation. The models [67,68] predict that the resistivity decreases with the increasing thickness until the bulk resistivity is reached, mainly due to the carriers scattering at the grains boundary and interfaces for low thicknesses.

In our case, due to the hopping transport mechanism, the interfaces scattering effect cannot be considered because the carrier hopping length is in the range of the lattice parameter (from copper site to an other neighbor copper site) and clearly negligible in comparison with

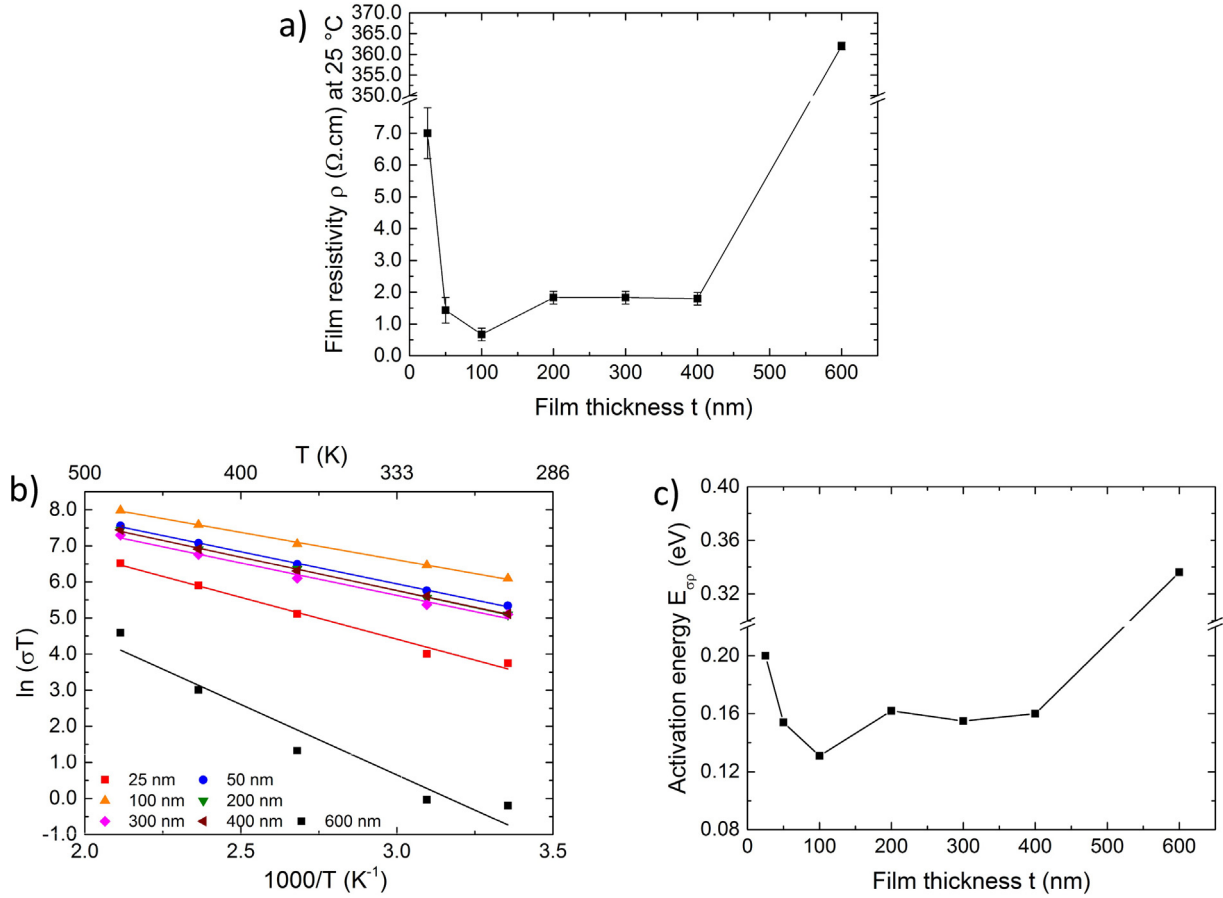


Fig. 4. (a) Film resistivity of the annealed $\text{CuCrO}_2:\text{Mg}$ films at 25 °C as a function of the film thickness. (b) Arrhenius plot. (c) Activation energy versus film thickness.

the thin film thickness. It is more probable that the grain boundaries impact the hopping transport by adding potential barriers that are multiplied at low thickness for which the grain size is very small (Fig. 2a).

For small thicknesses, the contribution of a lower carrier density determined by the Seebeck measurement, can partially explain the high electrical resistivity. Nevertheless, for the 25 nm thick film, the calculated macroscopic mobility ($\mu_{\text{hop}} = 2.32 \times 10^{-2} \text{ cm}^2 \text{ V}^{-1} \text{ s}^{-1}$), which is obtained using the Eq. (3), is lower than the value calculated for 100 nm thick film ($\mu_{\text{hop}} = 7.43 \times 10^{-2} \text{ cm}^2 \text{ V}^{-1} \text{ s}^{-1}$). These low value of the mobility explain the difficulty of performing the DC Hall measurement on this material as reported in [35].

$$\sigma = pe\mu_{\text{hop}} \quad (3)$$

where the hole density (p) is deduced from Heikes relation.

In the case of the small polaron hopping mechanism thermally activated, the mobility can be express according to the Mott's conductors [69] as:

$$\mu_{\text{hop}} = \frac{efd^2}{nk_B T} \exp(-2\phi d) \times \exp\left(\frac{-E_a}{k_B T}\right) \quad (4)$$

where f is the hopping frequency, d the average distance between two copper sites, T the temperature, ϕ the inverse of the decay length of the localized wave function, E_a the activation energy which is the required energy for the polaron to hop from a site to another and n a constant parameter which depends of the dimension for the hop ($n = 2$ in the case of linear chain hopping, $n = 4$ for 2D hopping and $n = 6$ for 3D hopping). In the case of $\text{CuCrO}_2:\text{Mg}$, we can suppose that the effective hopping is done only along the a and b axis (the CrO_6 octahedron along the c axis can be considerate as a barrier for the hole hopping) which corresponds to a 2D hopping transport mechanism.

In this case, only d and/or E_a are the parameters that can modify the global hopping mobility. Even if a variation of d can be caused by the lattice deformation due to the tensile stress [69], however from the GIXRD analysis (Fig. 1b), the variation of the $d_{(012)}$ remains very low ($< 0.4\%$) in the whole thickness range and cannot explain the large change of the mobility according to the Eq. (4). Therefore, the most probable cause of the mobility variation is the change of the activation energy. It can be due to an increase of the number of potential barrier that are located at the grain boundaries [70] for very small grains, which is observed in low thickness films (Fig. 2a). This is consistent with the experimental hopping activation energies (Fig. 4c) extracted from the Arrhenius plot [7,36,71], $\ln \sigma T = f(1/T)$, for various thicknesses (Fig. 4b).

Above 100 nm, the electrical resistivity increases which is unexpected. This variation cannot be attributed to the hole density decrease because the Seebeck coefficient measurement have shown that this value remains constant when the thickness increases over 100 nm. Thus, this can be only explained by a hopping mobility decrease due to stress effect [72] which are revealed by the micro cracks apparition in the thicker film (Fig. 2b and c).

In conclusion, due to microstructural and stress/strain effects, $\text{CuCrO}_2:\text{Mg}$ does not follow the classical models proposed for thin films and shows an optimal thickness for the electrical properties.

3.2.3. Thermoelectric properties analysis

From the measured Seebeck coefficient and the electrical conductivity, the thermoelectric power factor (PF) was calculated for various thicknesses at three different temperatures. It is plotted in the Fig. 5b and has been used to evaluate the performance of the thermoelectric thin films. As shown in the Fig. 5b, the PF increased with the measuring temperature. For the optimum thickness, 100 nm, the PF was

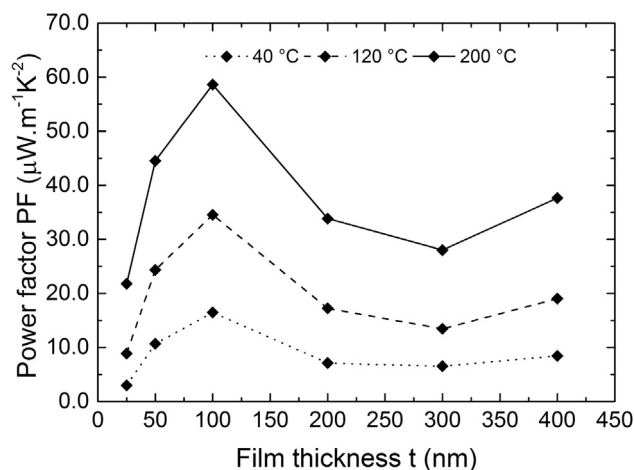


Fig. 5. Power factor versus film thickness for three different temperatures.

$59 \mu\text{W}\cdot\text{m}^{-1} \text{K}^{-2}$ at 200°C . Nevertheless, the obtained value of PF remains lower than the PF of Mg doped CuCrO_2 in bulk form published by Hayashi et al. [39] ($56 \mu\text{W}\cdot\text{m}^{-1} \text{K}^{-2}$ at 40°C) and Meng et al. [43] ($65 \mu\text{W}\cdot\text{m}^{-1} \text{K}^{-2}$ at 40°C). However, these authors announced that the PF doubled from 40 to 200°C in bulk form but in the present work, the 100 nm thick Mg doped film showed the PF nearly four times higher at 200°C than at 40°C . The stronger increase of the PF with the temperature in thin films provides a great interest to furthermore study. Moreover, thin films could have the figure of merit values higher than bulk thanks to the low substrate thermal conductivity ($\kappa_{\text{(fused silica)}} = 1.38 \text{ Wm}^{-1} \text{K}^{-1}$ [73]).

4. Conclusion

$\text{CuCrO}_2\text{:Mg}$ thin films with various thicknesses were deposited using RF magnetron sputtering and then annealed at 550°C under vacuum in order to form delafossite structure. An increase of the grain size is observed with AFM when the thickness is increased. Seebeck coefficient measurement showed highly degenerated semiconductor behavior for whole studied thicknesses and was thickness dependent. It decreased from 25 nm to 100 nm then it was stabilized for films thicknesses above 100 nm . Some proposed hypotheses are: a lattice deformation due to tensile stress effect and an incomplete crystallization causing a decrease of the carrier density at low thickness. The consequence was an increase of the film resistivity when the thickness decreases from 100 nm to 25 nm . The evolution of the resistivity in the whole thickness range was also related to the change in the hole mobility. From the calculated PF, we found that the optimum thickness for a highest thermoelectric performance was 100 nm with an electrical conductivity of $1.7 \text{ S}\cdot\text{cm}^{-1}$ and a Seebeck coefficient of $307 \mu\text{V}\cdot\text{K}^{-1}$, both at 40°C . The power factor attained $59 \mu\text{W}\cdot\text{m}^{-1} \text{K}^{-2}$ at 200°C . By thickness optimization, the electrical conductivity was increased without a negative impact on the Seebeck coefficient. This study reveals that the model and theories predict the influence of the thickness on physical properties but do not consider several parameters such as stress/strain and micro cracks which can affect strongly these properties.

Acknowledgements

The authors would like to thank the French ministry of Research for the National PhD funding.

References

- [1] F.A. Benko, F.P. Koffyberg, Preparation and opto-electronic properties of semi-conducting CuCrO_2 , *Mater. Res. Bull.* 21 (1986) 753–757.
- [2] R. Nagarajan, N. Duan, M.K. Jayaraj, J. Li, K.A. Vanaja, A. Yokochi, A. Draeseke, J. Tate, A.W. Sleight, p-Type conductivity in the delafossite structure, 3 (2001) 265–270.
- [3] a.N. Banerjee, K.K. Chattopadhyay, Recent developments in the emerging field of crystalline p-type transparent conducting oxide thin films, *Prog. Cryst. Growth Charact. Mater.* 50 (2005) 52–105. 10.1016/j.pcrysgrow.2005.10.001.
- [4] A. Stadler, Transparent conducting oxides-an up-to-date overview, *Materials (Basel)*. 5 (2012) 661–683.
- [5] A. Barnabé, Y. Thimont, M. Lalanne, L. Presmanes, P. Tailhades, P-type conducting transparent characteristics of delafossite Mg-doped CuCrO_2 thin films preparation by RF-sputtering, *J. Mater. Chem. C*. 3 (2015) 6012–6024.
- [6] K.H.L. Zhang, K. Xi, M.G. Blamire, R.G. Egdell, P type transparent conducting oxides, *J. Phys. Condens. Matter*. 28 (2016) 383002.
- [7] L. Farrell, E. Norton, C.M. Smith, D. Caffrey, I.V. Shvets, K. Fleischer, Synthesis of nanocrystalline Cu deficient CuCrO_2 – a high figure of merit p-type transparent semiconductor, *J. Mater. Chem. C*. 126 (2016) 126–134.
- [8] S. Gotzendorfer, R. Bywalez, P. Lobmann, Preparation of p-type conducting transparent CuCrO_2 and $\text{CuAlO}_2\text{Cr}_{0.5}\text{O}_2$ thin films by sol-gel processing, *J. Sol-Gel Sci. Technol.* 52 (2009) 113–119.
- [9] F. Lin, C. Gao, X. Zhou, W. Shi, A. Liu, Magnetic, electrical and optical properties of p-type Fe-doped CuCrO_2 semiconductor thin films, *J. Alloys Compd.* 581 (2013) 502–507.
- [10] R.S. Yu, D.H. Hu, Formation and characterization of p-type semiconductor CuCrO_2 thin films prepared by a sol-gel method, *Ceram. Int.* 41 (2015) 9383–9391.
- [11] H. Chen, J. Wu, C. Huang, Development of a fast annealing process to prepare transparent conductive Mg-doped CuCrO_2 thin films, *Thin Solid Films*. 605 (2016) 180–185.
- [12] P. Lunca Popa, J. Crépellière, R. Leturcq, D. Lenoble, Electrical and optical properties of Cu–Cr–O thin films fabricated by chemical vapour deposition, *Thin Solid Films*. 612 (2016) 194–201.
- [13] P. Barquinha, R. Martins, L. Pereira, E. Fortunato, Transparent oxide electronics : from materials to devices, John Wiley & Sons, Wiley, 2008.
- [14] J.F. Wager, D.A. Kesler, D.A. Presley, Transparent Electronics, Springer, 2008.
- [15] K. Tonooka, N. Kikuchi, Preparation of transparent CuCrO_2 : Mg/ZnO p-n junctions by pulsed laser deposition, *Thin Solid Films*. 515 (2006) 2415–2418.
- [16] T.W. Chiu, K. Tonooka, N. Kikuchi, Fabrication of ZnO and CuCrO_2 : Mg thin films by pulsed laser deposition in situ laser annealing and its application to oxide diodes, *Thin Solid Films*. 516 (2008) 5941–5947.
- [17] J. Tate, M.K.K. Jayaraj, A.D.D. Draeseke, T. Ulbrich, A.W.W. Sleight, K.A.a. Vanaja, R. Nagarajan, J.F.F. Wager, R.L.L. Hoffman, p-Type oxides for use in transparent diodes, *Thin Solid Films* 411 (2002) 119–124.
- [18] M. Asemi, M. Ghanaatshoar, Hydrothermal growth of one-dimensional Ce-doped TiO_2 nanostructures for solid-state DSSCs comprising Mg-doped CuCrO_2 , *J. Mater. Sci.* 52 (2017) 489–503.
- [19] S. Powar, D. Xiong, T. Daeneke, M.T. Ma, A. Gupta, G. Lee, S. Makuta, Y. Tachibana, W. Chen, L. Spiccia, Y.-B. Cheng, Improved photovoltages for p-Type dye-sensitized solar cells using CuCrO_2 nanoparticles, *J. Phys. Chem. C*. 118 (2014) 16375–16379.
- [20] A. Wuttig, J.W. Krizan, J. Gu, J.J. Frick, R.J. Cava, A.B. Bocarsly, The effect of Mg-doping and Cu nonstoichiometry on the photoelectrochemical response of CuFeO_2 , *J. Mater. Chem. A*. 5 (2017) 165–171.
- [21] K. Toyoda, R. Hinogami, N. Miyata, M. Aizawa, Calculated descriptors of catalytic activity for water electrolysis anode: application to delafossite oxides, *J. Phys. Chem. C*. 119 (2015) 6495–6501.
- [22] W. Ketir, R. Rekhila, M. Trari, A. Amrane, Preparation, characterization and application of $\text{CuCrO}_2\text{/ZnO}$ photocatalysts for the reduction of Cr(VI), *J. Environ. Sci.* 24 (2012) 2173–2179.
- [23] S. Saadi, A. Bouguelia, M. Trari, Photocatalytic hydrogen evolution over CuCrO_2 , *Sol. Energy*. 80 (2006) 272–280.
- [24] R. Rao, A. Dandekar, R.T.K. Baker, M.A. Vannice, Properties of copper chromite catalysts in hydrogenation reactions, *J. Catal.* 171 (1997) 406–419.
- [25] W. Ketir, A. Bouguelia, M. Trari, Visible light induced NO_2 (-) removal over CuCrO_2 catalyst, *Water Air Soil Pollut.* 199 (2009) 115–122.
- [26] P. Zhang, Y. Shi, M. Chi, J.N. Park, G.D. Stucky, E.W. McFarland, L. Gao, Mesoporous delafossite CuCrO_2 and spinel Cu_2O_4 : synthesis and catalysis, *Nanotechnology* 24 (345704) (2013) 1–8.
- [27] T.W. Chiu, Y.C. Yang, A.C. Yeh, Y.P. Wang, Y.W. Feng, Antibacterial property of CuCrO_2 thin films prepared by RF magnetron sputtering deposition, *Vacuum* 87 (2013) 174–177.
- [28] J. Patzsch, I. Balog, P. Krauß, C.W. Lehmann, J.J. Schneider, Synthesis, characterization and p-n type gas sensing behaviour of CuFeO_2 delafossite type inorganic wires using Fe and Cu complexes as single source molecular precursors, *RSC Adv.* 4 (2014) 15348.
- [29] E. Elgazzar, A. Tataroglu, A.A. Al-Ghamdi, Y. Al-Turki, W.A. Farooq, F. El-Tantawy, F. Yakuphanoglu, Thermal sensors based on delafossite film/p-silicon diode for low-temperature measurements, *Appl. Phys. A*. 122 (2016) 617.
- [30] X.G. Zheng, K. Taniguchi, A. Takahashi, Y. Liu, C.N. Xu, Room temperature sensing of ozone by transparent p-type semiconductor CuAlO_2 , *Appl. Phys. Lett.* 85 (2004) 1728–1729.
- [31] S. Zhou, X. Fang, Z. Deng, D. Li, W. Dong, R. Tao, G. Meng, T. Wang, Room temperature ozone sensing properties of p-type CuCrO_2 nanocrystals, *Sensors Actuators B*. 143 (2009) 119–123.
- [32] J. Shu, X. Zhu, T. Yi, CuCrO_2 as anode material for lithium ion batteries, *Electrochim. Acta*. 54 (2009) 2795–2799.
- [33] A.K. Díaz-García, T. Lana-Villarreal, R. Gómez, Sol-gel copper chromium delafossite thin films as stable oxide photocathodes for water splitting, *J. Mater. Chem. A*. 3 (2015) 19683–19687.
- [34] C. Taddee, T. Kamwanna, V. Amornkitbamrung, Characterization of transparent

- superconductivity Fe-doped CuCrO_2 delafossite oxide, *Appl. Surf. Sci.* 380 (2016) 237–242.
- [35] M. O'Sullivan, P. Stamenov, J. Alaria, M. Venkatesan, J.M.D. Coey, Magnetoresistance of CuCrO_2 -based delafossite films, *J. Phys. Conf. Ser.* 200 (052021) (2010) 1–4.
- [36] A. Maignan, C. Martin, R. Frésard, V. Eyert, E. Guilmeau, S. Hébert, M. Poienar, D. Pelloquin, S. Hébert, M. Poienar, D. Pelloquin, On the strong impact of doping in the triangular antiferromagnet CuCrO_2 , *Solid State Commun.* 149 (2009) 962–967.
- [37] R. Hoffman, J. Wager, Transistor device having a delafossite material, United States Pat. 7 026 713 (2006).
- [38] E. Guilmeau, A. Maignan, C. Martin, Thermoelectric oxides: effect of doping in delafossites and zinc oxide, *J. Electron. Mater.* 38 (2009) 1104–1108.
- [39] K. Hayashi, K.I. Sato, K. Nozaki, T. Kajitani, Effect of doping on thermoelectric properties of delafossite-type oxide CuCrO_2 , *Jpn. J. Appl. Phys.* 57 (2008) 59–63.
- [40] Y. Ono, K. Satoh, T. Nozaki, T. Kajitani, Structural, magnetic and thermoelectric properties of delafossite-type oxide, $\text{CuCr}_{1-x}\text{Mg}_x\text{O}_2$ ($0 \leq x \leq 0.05$), *Jpn. J. Appl. Phys.* 46 (2007) 1071–1075.
- [41] T. Okuda, N. Jufuku, S. Hidaka, N. Terada, Magnetic, transport, and thermoelectric properties of the delafossite oxides $\text{CuCr}_{1-x}\text{Mg}_x\text{O}_2$ ($0 \leq x \leq 0.04$), *Phys. Rev. B.* 72 (2005) 144403.
- [42] T.N.M. Ngo, T.T.M. Palstra, G.R. Blake, Crystallite size dependence of thermoelectric performance of CuCrO_2 , *RSC Adv.* 6 (2016) 91171–91178.
- [43] Q. Meng, S.S. Lu, S.S. Lu, Y. Xiang, Preparation of p-type $\text{CuCr}_{1-x}\text{Mg}_x\text{O}_2$ bulk with improved thermoelectric properties by sol-gel method, *J. Sol-Gel Sci. Technol.* 63 (2012) 1–7.
- [44] C. Ruttanapun, S. Maensiri, Effects of spin entropy and lattice strain from mixed-trivalent $\text{Fe}^{3+}/\text{Cr}^{3+}$ on the electronic, thermoelectric and optical properties of delafossite $\text{CuFe}_{1-x}\text{Cr}_x\text{O}_2$, *J. Phys. D. Appl. Phys.* 48 (2015) 495103.
- [45] C. Bianchi, J. Loureiro, P. Duarte, J. Marques, J. Figueira, I. Ropio, I. Ferreira, V_2O_5 Thin films for flexible and high sensitivity transparent temperature sensor, *Adv. Mater. Technol.* 1 (2016) 1600077.
- [46] M. Ruoho, T. Juntunen, T. Alasaarela, M. Pudas, I. Tittonen, M. Ruoho, T. Juntunen, T. Alasaarela, I. Tittonen, M. Pudas, Transparent, flexible and passive thermal touch panel, *Adv. Mater. Technol.* 1 (2016) 2365–2709.
- [47] C. Bianchi, L.M. Ferreira, J. Loureiro, A. Rodrigues, P. Duarte, A.C. Baptista, I.M. Ferreira, Vanadium pentoxide alloyed with graphite for thin-film thermal sensors, *J. Electron. Mater.* 45 (2016) 1987–1991.
- [48] R. Venkatasubramanian, Thin-film thermoelectric cooling and heating devices for DNA genomic and proteomic chips, thermo-optical switching circuits, and IR tags, *US 7164077 B2*, 2007.
- [49] W. Glatz, C. Hierold, Flexible micro thermoelectric generator, in: 2007 IEEE 20th Int. Conf. Micro Electro Mech. Syst., IEEE, 2007: pp. 89–92.
- [50] M. Ruoho, T. Juntunen, I. Tittonen, Large-area thermoelectric high-aspect-ratio nanostructures by atomic layer deposition, *Nanotechnology* 27 (2016) 355403.
- [51] S. Ali, T. Juntunen, S. Sintonen, O.M.E. Ylivaara, R.L. Puurunen, H. Lipsanen, I. Tittonen, S.-P. Hannula, Thermal conductivity of amorphous $\text{Al}_2\text{O}_3/\text{TiO}_2$ nanolaminates deposited by atomic layer deposition, *Nanotechnology* 27 (2016) 445704.
- [52] S.H. Choday, M.S. Lundstrom, K. Roy, Prospects of thin-film thermoelectric devices for hot-spot cooling and on-chip energy harvesting, *IEEE Trans. Components, Packag. Manuf. Technol.* 3 (2013) 2059–2067.
- [53] J.H. Kiely, D. Lee, Characteristics of $\text{Bi}_2\text{O}_3\text{Sb}_2\text{Te}_3/\text{Be}_2\text{Te}_2\text{Se}_2$ thin film thermoelectric devices for power generation, *Measurement Sci. Technol.* 8 (1997) 661–665.
- [54] R. Venkatasubramanian, E. Siivola, T. Colpitts, B. O'Quinn, Thin-film thermoelectric devices with high room-temperature figures of merit, *Nature.* 413 (2001) 597–602.
- [55] D.G. Cahill, H.E. Fischer, T. Klitsner, E.T. Swartz, R.O. Pohl, Thermal conductivity of thin films: Measurements and understanding, *J. Vac. Sci. Technol. A Vacuum, Surfaces, Film.* 7 (1989) 1259.
- [56] J. Loureiro, J.R. Santos, A. Nogueira, F. Wyczisk, L. Divay, S. Reparaz, F. Alzina, C.M. Sotomayor Torres, J. Cuffe, F. Montemor, R. Martins, I. Ferreira, Nanostructured p-type $\text{Cr}/\text{V}_2\text{O}_5$ thin films with boosted thermoelectric properties, *J. Mater. Chem. A.* 2 (2014) 6456.
- [57] R. Venkatasubramanian, E. Siivola, B. O'Quinn, K. Coonley, T. Colpitts, P. Addepalli, M. Napier, M. Mantini, Nanostructured Superlattice Thin-Film Thermoelectric Devices, *Nanotechnol. Environ.* 2004: pp. 347–352.
- [58] K. Koumoto, Y. Wang, R. Zhang, A. Kosuga, R. Funahashi, Oxide thermoelectric materials: a nanostructuring approach, *Annu. Rev. Mater. Res.* 40 (2010) 363–394.
- [59] D.K. Aswal, R. Basu, A. Singh, Key issues in development of thermoelectric power generators: High figure-of-merit materials and their highly conducting interfaces with metallic interconnects, *Energy Convers. Manag.* 114 (2016) 50–67.
- [60] Z.-G. Chen, G. Han, L. Yang, L. Cheng, J. Zou, Nanostructured thermoelectric materials: current research and future challenge, *Prog. Nat. Sci. Mater. Int.* 22 (2012) 535–549.
- [61] I. Sinnarasa, Y. Thimont, L. Presmanes, A. Barnabé, P. Tailhades, Thermoelectric and Transport Properties of Delafossite $\text{CuCrO}_2:\text{Mg}$ Thin Films Prepared by RF Magnetron Sputtering, *Nanomater.* 2017, Vol. 7, Page 157. 7 (2017) 157.
- [62] H. Le Trong, T.M.A. Bui, L. Presmanes, A. Barnabé, I. Pasquet, C. Bonningue, P. Tailhades, Preparation of iron cobaltite thin films by RF magnetron sputtering, *Thin Solid Films.* 589 (2015) 292–297.
- [63] R. Nagarajan, A.D. Draeseke, A.W. Sleight, J. Tate, P-type conductivity in $\text{CuCr}_{1-x}\text{Mg}_x\text{O}_2$ films and powders, *J. Appl. Phys.* 89 (2001) 8022.
- [64] K. Geoffrey, Thermal expansion of glasses at low temperatures, *Retrospect. Theses Diss.* (1978) 6571.
- [65] R. Bywalez, S. Götzendörfer, P. Löbmann, Structural and physical effects of Mg-doping on p-type CuCrO_2 and CuAlO_2 thin films, *J. Mater. Chem.* 20 (2010) 6562–6570.
- [66] P. Lunca Popa, J. Crépellière, P. Nukala, R. Leturcq, D. Lenoble, Invisible electronics: metastable Cu-vacancies chain defects for highly conductive p-type transparent oxide, *Appl. Mater. Today.* 9 (2017) 184–191.
- [67] A.F. Mayadas, M. Shatzkes, Electrical-resistivity model for polycrystalline films: the case of arbitrary reflection at external surfaces, *Phys. Rev. B.* 1 (1970) 1382–1389.
- [68] A.F. Mayadas, R. Feder, R. Rosenberg, Resistivity and structure of evaporated aluminum films, *J. Vac. Sci. Technol.* 6 (1969) 690–693.
- [69] N.F. Mott, Conduction in non-crystalline materials, *Philosophical Magazine* 19 (160) (1969) 835–852.
- [70] S. Tsurekawa, K. Kido, T. Watanabe, Measurements of potential barrier height of grain boundaries in polycrystalline silicon by Kelvin probe force microscopy, *Philos. Mag. Lett.* 85 (2005) 41–49.
- [71] D.O. Scanlon, G.W. Watson, K. et al. Hayashi, Understanding the p-type defect chemistry of CuCrO_2 , *J. Mater. Chem.* 21 (2011) 3655.
- [72] A. Fluri, D. Pergolesi, V. Roddatis, A. Wokaun, T. Lippert, In situ stress observation in oxide films and how tensile stress influences oxygen ion conduction, *Nat. Commun.* 7 (2016) 10692.
- [73] P. Combis, P. Cormont, L. Gallais, D. Hebert, L. Robin, J.-L. Rullier, Evaluation of the fused silica thermal conductivity by comparing infrared thermomasurements with two-dimensional simulations, *Appl. Phys. Lett.* 101 (2012) 211908–264319.